Aerostructural Design of a Medium-Altitude Medium-Endurance UAV Wing

Pedro Marques Cardoso
pedro.marques.cardoso@tecnico.ulisboa.pt

Instituto Superior Técnico, Universidade de Lisboa, Portugal

December 2024

Abstract

In a competitive market, manufacturers strive to enhance UAV performance through advanced design technologies. This study focuses on maximizing UAV range by optimaly designing the wing with the aerostructural, gradient-based framework, MACH, integrating high-fidelity computational models. The process optimizes aerodynamic and structural variables like chord, airfoil, span, panel thickness and composite fiber orientation, using the discrete adjoint method for efficient derivative computation. Single-discipline optima were studied to establish a baseline for the aerostructural problem. The impact of higher-fidelity geometry wing models was examined through aerostructural analysis of a simplified wing, a detailed wing, and a wing-fuselage group, revealing aspects missed in single-discipline analyses, including the impact of structural twist in the aerodynamic response. Manufacturing constraints in multilayer composites, including neighboring ply angle adjacency and orthogonality, had minimal impact. However, the tip displacement constraint affected significantly the aerodynamic airfoil variable and final designs. Exploring the response at dive speed for a more flexible wing showed promising results. Comparing aerostructural and single-discipline optimizations, highlighted the computational intensity of the former but superior design outcomes, including extended range achieved by root-heavy and tip-light thickness, and lift distribution. Addressing both aerodynamic and structural disciplines concurrently offers valuable insights into trade-offs among design variables. Compered to baseline wing design final optimal showed from 4.2% increase in range with a 10.4% gain in aerodynamic efficiency and 43.9% reduction in mass, up to 9.9% increase in range if span was a variable, with a 32% improvement in aerodynamic efficiency, despite a 114% increase in wing weight.
Keywords: multidisciplinary optimization, fluid-structure interaction, wing design, adjoint method, free-form deformation, composite materials

1. Introduction

The landscape of Unmanned Aerial Vehicles (UAVs) has evolved rapidly, being the competition among manufacturers is increasingly fierce. To address this study focuses on the enhancement of the TEKEVER AR5 to strengthen its competitive edge in the Medium-Altitude Medium-Endurance (MAME) fixed-wing UAV sector. This UAV model is designed to execute a variety of missions, as search and rescue, maritime surveillance and patrol, offering advantages in extended endurance and cost-effective operation. Its key specifications are cruise speed of 30 m/s at 305 m altitude, with a takeoff weight of 170 kg, wing span of 7.3 m and 2.17 m^2 wing area.

The primary objective is to improve the wing of the AR5, enhancing its aerodynamic efficiency and structural integrity. Considering that the wing is a flexible structure, whose shape differs significantly under loads in flight due to fluid-structure interactions, a high-fidelity aerostructural design tool is employed [1]. This study is a follow up of in wing aerodynamically [2] and structurally [3] individual optimized.

2. Aerostructural Design Framework

The aerostructural design framework used was developed by the Multidisciplinary Design Optimization (MDO) Laboratory at the University of Michigan [4] and includes three main stages, as depicted in Fig. 1.

2.1. Pre-processing stage

Based on the geometry CAD description of the TEKEVER AR5 wing, the aerodynamic mesh is created. Starting by the creation of surface mesh characterized by its high density at the leading, trailing edge and wing tip [2] and sharp edges are avoidance consistent with being a based for hyperbolic strutted volume mesh. The next step is the

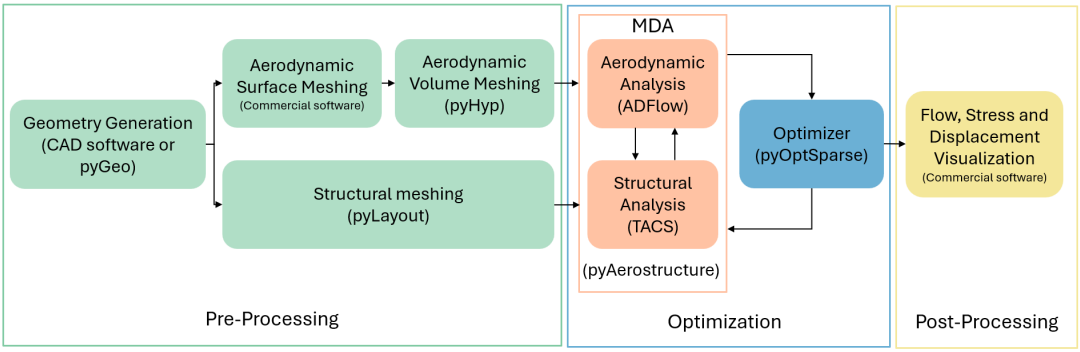

Figure 1: MACH-Aero aerostructural design framework

volume mesh generation using `pyHyp` [5], achieving the general topology observed in Fig 2a, which also applies the far-field and wall boundary conditions. The first layer height was prescribed, and latter verified to guarantee a y+ close to unity as required by the Spalart-Allmaras turbulence model employed, chosen for its effectiveness at predicting the turbulent effect around the wing at the AR5 operating conditions and for being differentiated in the MACH-Aero framework [6]. A mesh refinement study concluded that 800,000 cells were sufficient, considering the trade-off between accuracy and performance, with 0.5% difference in lift and 5% drag but converged in only 20% of the time, compared to the most refined mesh studied. The computational domain extends 15 chords [2].

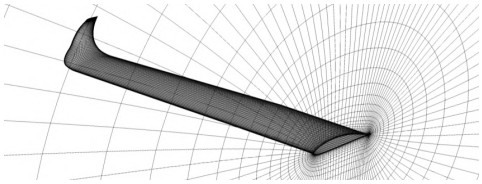

(a) Aerodynamic volume mesh

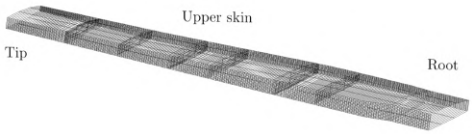

(b) Structural mesh

Figure 2: Computational meshes of TEKEVER AR5 wing

To avoid the computational burden of generating new meshes from scratch, the Free-Form Deformation (FFD) method is employed, which is based on generating boxes through control points surrounding the wing surface, then when moved modify the wing geometry [7]. Although each point can be individually moved, as done in airfoil shape optimization, it is more practical to reduce and create aggregated as parametric global variables like chord, twist, and span [8]. In MACH-Aero, `pyGeo` is the module responsible for performing this task; moreover, it also handles the computation of the global DV derivatives using the chain rule [8].

The structural finite element mesh is generated with `pyLayout`, an automated module for the creation of wingbox structures for wings. When given a CAD file along with the position of spars and ribs generates the structural layout, as shown in Fig. 2b. Since these wing parts are thin and made of fibre-reinforced composite materials, bilinear, 4-node, 2-D shell elements were used [3, 9]. From a mesh convergence study monitoring the tip displacement and average stress, a mesh with 1,000,000 DoF was selected, which presents an error smaller than 2% in both parameters [3].

2.2. Optimization stage

The Multidisciplinary Feasible (MDF) MDO architecture is used for its simplicity and accuracy at the optimizer level [1]. The problem is solved as a single discipline where the couple results are given by a Multidisciplinary Analysis (MDA). This methodology allows for the use of the previously developed, fully differentiated aerodynamic and structural solvers [10].

The aerodynamic discipline is solved using `ADFLOW` [6] and the structural discipline is solved using `TACS` [11]. `ADFLOW` employs a finite-volume method to solve the steady compressible RANS equations, utilizing the Spalart-Allmaras model for turbulence. The models' discretization relies on central finite differences with JST scalar dissipation. As `ADFLOW` is a compressible flow solver and the TEKEVER AR5 operates at very low Mach number, the solver uses characteristic time-stepping combined with an approximate Newton method, and the van Leer-Lee-Roe preconditioner to enhance both accuracy and convergence. Convergence is defined by achieving a 10^{-6} reduction in the L2-norm of the residual. Default settings

are used for all other solver settings [6]. `TACS` is finite-element solver and computes the generalized Hooke's Law [12]. The material is considered orthotropic, with the fibres parallel within a ply, allowing the rule of mixtures [13]. The failure criteria is the Tsai-Wu [14].

The disciplines are coupled using `pyAerostructure`, which captures the interactions between aerodynamic forces and structural displacements [1]. The MDA is converged using Gauss-Seidel with tolerance set to 10^{-5}. The displacements are transferred between the meshes through using the Rigid Link Transfer (RLT) (Fig: 3) technique [1], and the method of virtual work is used to determine the structural nodal forces [1] given by the integration of the aerodynamic loads.

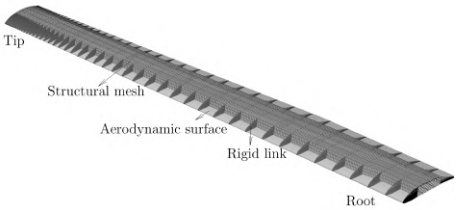

Figure 3: Overlay of the rigid links, structural and aerodynamic mesh

The wing volume mesh is deformed at each aerostructural iteration during using an Inverse-Distance Weighting method (IDW) [5].

The gradient-based SLSQP algorithm is used in the optimization process itself, that proved to be adequate in similar problems [15]. The module `pyOptSparse` [16] implements such constrained optimizer.

The sensitivity analysis, required for the search direction evaluation in the gradient-based optimizer, is efficiently and accurately performed using the adjoint method, since there are considerably more design variables than metric functions [17]. The coupled system of adjoint equations is treated as a unified problem, solving the entire set together to directly address the interdependencies between different disciplines, leading to more accurate sensitivity analysis and faster convergence [1]. The adjoint solver is converged using the Krylov subspace approach, with a tolerance of 10^{-5}.

To prevent material failure, the Kreisselmeier-Steinhauser (KS) aggregation technique is used [12], which provides a smooth estimate of the maximum stress, while avoiding issues of discontinuity and excessive constraints.

3. Multidisciplinary Analysis

The wing deformation in the aerostructural analysis results in a change of its aerodynamic shape and incidence angle, causing an increase in lift for high angles-of-attack, delaying and smoothing the stall condition while at lower angles the attack the effect is the reverse (shift in the relation between the elastic and pressure center) aspect that could not be observe in the single discipline analysis This reveals that the aerostructural coupling is significant and must accounted for in the wing design. Additionally, it also highlights that there is an adverse bending-twist behavior in the baseline wing.

The aerodynamic shape comparison between the two models is illustrated in Fig. 4, reinforcing the strong fluid-structure interaction.

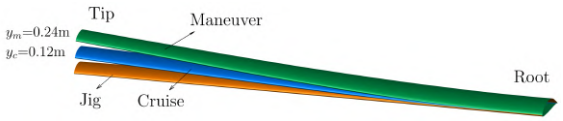

Figure 4: Comparison between rigid and elastic wing model

The effect of a more detailed aerodynamic wing shape considering the winglet and the fuselage was also studied. Fig. 5b) demonstrates the large decrease in drag around the winglet showcasing its importance in obtaining an efficient solution. Moreover,the fuselage creating interference drag around the locking point, showcased in Fig. 5b). The lift in that region also reduces compared to the simple wings analysis (Fig. 5a)), that will affect the preceded optimal solution, considering that in an aerostructural analysis the wing root is of great importance, due to the expected structural discipline influence.

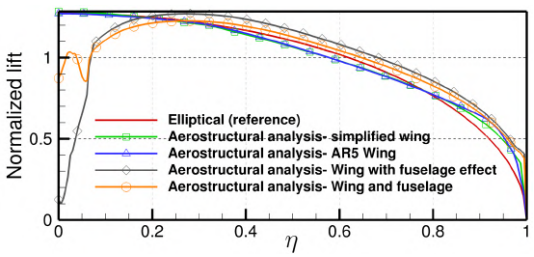

(a) Lift distribution

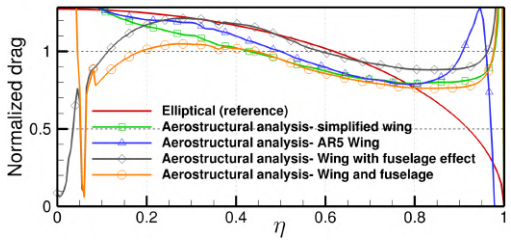

(b) Drag distribution

Figure 5: Comparison between the different wing fidelity levels

4. Single Disciplinary Optimization

A preliminary aerodynamic single optimization, led to a 4.76% reduction in drag, at fixed lift, primarily due to airfoil thinning, which was constrained by structural concerns, and an winglet height increase. A specific winglet optimization showed a reduced drag by 2.5%, achieved through small adjustments in twist, chord, and large increase in winglet dihedral values.

The structural optimization achieved a 43.6% reduction in wing mass, but at the cost of a 137% increase in wing deflection. These results showcased the need for additional constraints, particularly to limit displacement and control wing torsion in the individual solution.

5. Multidisciplinary Optimization

The aerostructural optimization targets the maximization of the aircraft range R defined by the Breguet equation,

$$R = \frac{L}{D}\frac{\eta}{sfc \cdot g}\ln\left(\frac{W_0}{W_f}\right), \tag{1}$$

where the lift L and drag D depend on the aerodynamic performance, and the initial W_0 and final W_f weight depend on the structural performance, the remaining equation terms are fixed by flight operating condition, the propulsion efficiency η and specific fuel consumption sfc. g is the gravitational acceleration. Finally, the wing design variables (DV) are summarized in Tables 1 as angle of attack, twist and chord distribution, span, airfoil shape, and in Table 2 as material ply angles and structural thickness.

Table 1: Aerodynamic design variables

DV	α	γ	c	b	$shape$
Quantity	1	5	6	6	6x4
L. Bound	-4°	-15°	-1 m	1 m	-0.05 m
U. Bound	20°	15°	1.5 m	1.5 m	0.05 m

Table 2: Structural design variables

DV	θ_1/θ_2	t
Quantity	2N	N
L. Bound	0°	0.01 m
U. Bound	90°	0.1 m

The twist and chord distributions are functions of the wing spanwise coordinate. The shape DV is controlled by 4 points along the airfoil, along 7 section in the spanwise direction, where each of the control points has the freedom to move up and down, inside its bounds, changing the airfoil shape. The fibre angles and material thickness are defined for each block i of the N blocks presented in Fig. 6.

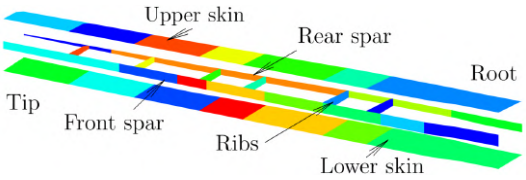

Figure 6: Wing structural blocks

The design must satisfy six requirements, included in the form of constraints in the optimization: i) the trimming of the aircraft implies that the lift generated must match the UAV weight at level flight, $L = W$; the structure must not fail under a 2-g manoeuvre, $KS(failure) \leq n(2g)$;iii the structure must not deflect more than $\Delta_{\max}$;iv) adjacency constraints to keep the difference in each design block thickness under a maximum threshold, $|t_i - t_{i+1}| \leq \Delta_{\max}$; v) composite ply angle continuity among consecutive blocks for manufacturability, $\theta_{1,i} = \theta_{1,i+1}$ and $\theta_{2,i} = \theta_{2,i+1}$; vi) orthogonality between plies for manufacturability to allow the use of carbon fibre cloths with weaving pattern, $|\,\theta_1 - \theta_2\,| = 90°$.

The wing aerostructural optimal design problem was posed in standard form as

$$\begin{aligned}
&\text{maximize} && R \\
&\text{with respect to} && \alpha, \gamma, c, b, shape, \theta_{1,i}, \theta_{2,i}, t_i \\
&\text{subject to} && L = W \\
& && KS(\text{failure}) \leq n(2g) \\
& && KS(\text{displacement}) \leq \Delta_{\max} \\
& && |t_i - t_{i+1}| \leq \Delta_{\max} \\
& && \theta_{1,i} = \theta_{1,i+1} \\
& && \theta_{2,i} = \theta_{2,i+1} \\
& && |\theta_1 - \theta_2| = 90°.
\end{aligned} \tag{2}$$

5.1. Effect of Manufacturing Constraints

Considering the simplified TEKEVER AR5 wing (without winglet) a first optimization was done without the two manufacturability constraints (v) and (vi). Overall, it achieved 0.6% increase in aerodynamic efficiency, 51.9% wing weight reduction and a 0.9% increase in range.

As expected, the optimizer did not to converge to the ideal aerodynamic elliptical lift distribution but rather increased the lift produced in the inner portion of the wing and reduced it closer to the tip, contributing to less bending moment, thus lighter structure and an improved coupled aerostructural solution. To achieve this lift distribution the optimizer significantly reduces wing twist in the middle (from 2° to 1.2°) and tip sections of the wing (from

0.5° to -4°). It also caused an improvement in structural efficiency, as attested by the increase in the KS index failure from an original maximum of around 0.1 to 0.35. The verified behavior occurred due to the significant thinning of panels, observed in Fig. 7, particularly at the front spar and lower skin panels.

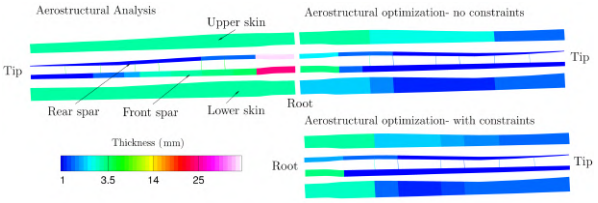

Figure 7: Thickness distribution with and without manufacturing constraints.

The ply angle distribution between the blocks is shown in Fig. 8. When the optimizer is given full freedom, the solution is non-monotonic distribution, which would make manufacturing difficult. The angle between plies not being 90° makes it impossible to use standard interwoven carbon fiber, increasing the cost. To address the issues described, the manufacturing constraints of adjacency ply angles (iv) and orthogonality (vi) were added.

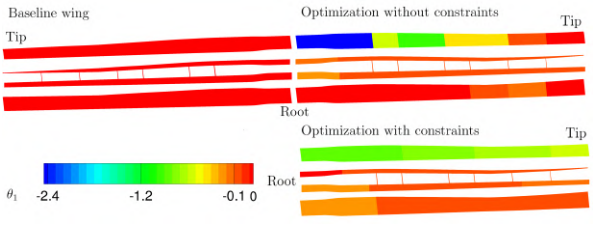

(a) Angle θ_1

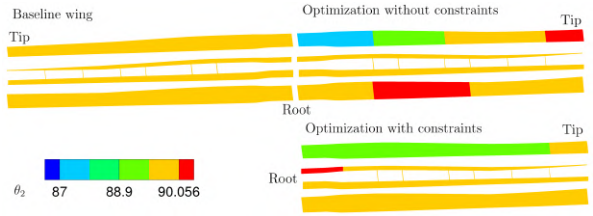

(b) Angle θ_2

Figure 8: Optimal distribution of ply angles with and without manufacturing constraints

Figure 8 demonstrates that the new optimal solution is now feasible in terms of manufacturing. This change did not affect the general optimized solution and respective structural and aerodynamic response, the failure index, final tip torsion (Fig: 7) and lift distribution are identical. Moreover, the general thickness distribution (Fig: 7) is also similar, however with a slight bump in the first lower skin panel is observed justifying the small increase in mass and reduction in range. With these additional constraints, the aircraft range increased 0.8% compared to the baseline, representing a small loss in relative to the previous non-manufacturing constrained case.

5.2. Effect off the Maximum Tip Deflection Constraint

Moreover, it was observed a very high deflection and tip torsion for twist, chord and shape case. Therefore it was established a maximum tip vertical deflection constraint at 0.13 normalized half-span. This resulted in a 4.2% increase in range, with a 10.4% increase in aerodynamic efficiency at an 5° angle of attack and 43.9% reduction in mass. This led to a 1.6% loss in range compared to the constrained case.

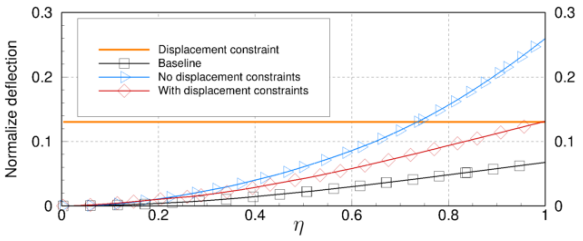

Figure 9: Wing deflection comparison with and without deflection constraints.

The wing deflection for the baseline, optimization with and without the maximum displacement constraint are depicted in Fig. 9. The constraint allowed for a reduction in deflection from 28% of half-span to 13%, as desired. This change in deflection was achieved by a smaller than the unconstrained case decrease in panel and spar thickness along the span, specially in the front spar and upper skin panel. These higher thicknesses together with a much thicker airfoil impose a much smaller failure index along the panels, reducing from a maximum of around 0.45 at the optimization without the maximum displacement constraint for a more in line with the remaining cases of 0.35, moreover, there more panels closer to failure (Fig. 10). The constrained case exhibits positive twist near the root

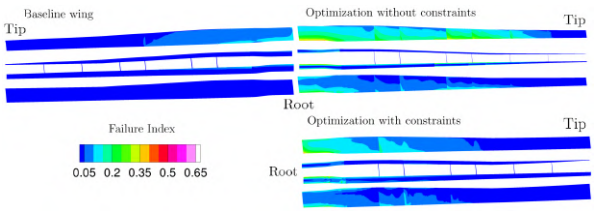

Figure 10: Failure index comparison for optimized twist, chord, and shape design variables: with and without deflection constraints.

and downwash at the tip. Moreover, the airfoil becomes more symmetric and thicker than in the unconstrained solution, especially near the wingtip, as shown in Tab. 3. This thicker airfoil strengthens the wing against bending moments. Moreover, the airfoil becomes more symmetric and thicker than in the unconstrained solution, especially near the wingtip, as shown in Table 3. This thicker airfoil strengthens the wing against bending moments, which drives the optimization toward a design closer to the baseline, however, with lower thickness at the tip than the arbitrary value constrained at aerodynamic optimum present at Section 5.4 (10%) but smaller in the remaining wing.

Table 3: Thickness comparison for optimized twist, chord, and shape design variables: with and without deflection constraints at 10%, 50% and 90% span.

	Baseline	Unconstrained	Constrained
t at 10%	ref	-37.0%	-8.1%
t at 50%	ref	-14.1%	-9.1%
t at 90%	ref	-46.4%	-14.1%

5.3. Effect of the Aerodynamic Design Variables

The effect that each design variable had in the final result was studied. For that, the following combinations cases where performed: twist; chord; span and twist; shape; twist, chord and shape (as span variation implied drastic modifications of the whole wing design); and all DVs including span to fully characterize the possibilities in the design. The main results are summarized in Tab. 4.

Table 4: Optimization results for the simplified TEKEVER AR5 wing as starting geometry.

Case	α	m	L/D	R
γ	2.4°	-50.6%	+0.6%	+0.8%
c	1.7°	-56.6%	+0.9%	+1.0%
γ, b	0°	+131.0%	+20.9%	+6.3%
Shape	2.3°	-42.3%	+10.6%	+4.5%
γ, c, *Shape*	2.5°	-47.0%	+14.4%	+5.8%
All DV	3.2°	+114%	+ 32.2%	+9.9%

The optimal lift distributions indicated that the optimizer did not achieve the ideal elliptical lift for any of the cases.

Instead, it increased lift near the wing root and reduced it near the tip for better structural loading at a various degrees (Fig. 11. With more aerodynamic variables as in the all DVs case, there was a shift towards overall aerodynamic efficiency. In the twist, chord and shape case, significant deflection was observed, prioritizing increased lift at the root and decreased lift at the tip for better structural loading.

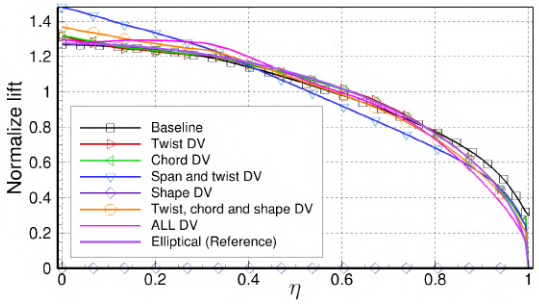

Figure 11: Lift distribution for each optimization case.

Using the chord design variable enables the optimizer to minimize weight by reducing the chord while pursuing an aerostructural lift optimum distribution. This is particularly clear in the all DVs case, where the increase in span and wing area needs to be balanced (Fig. 12).

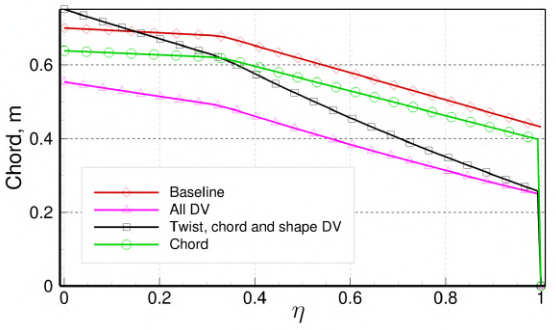

Figure 12: Chord distribution for each optimization case.

The elastic wing twist generally follows a consistent path (Fig. 13), where the twist decreases along the span. This twist behavior is beneficial for both aerodynamic and structural performance by shifting more lift toward the root of the wing, considering the angles of attack in Tab. 4 allow to obtain the effective angle of attack of the wing. When span is included as a design variable, the effect becomes more pronounced. A larger span increases the wing area, which requires a lower overall lift per section. In cruise conditions, a maximum tip twist of about -4° was observed for all design variables. Moreover, the applied washout, besides its advantages in drag reduction, is also a desirable safety feature to ensure that the root section stalls before the outer section, were control surfaces are located. The twist, shape, and chord optimization case presents an outlier where excessive structural flexibility related to torsion is observed.

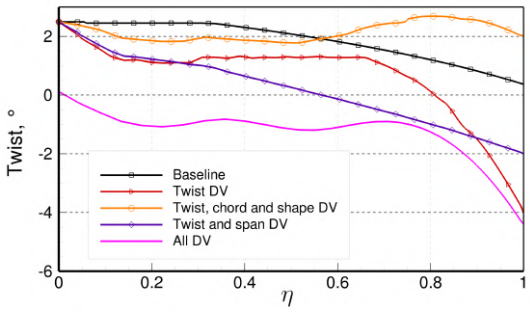

Figure 13: Effect of twist in aerostructural optimization.

The effect of the airfoil shape design variable can be seen in Fig. 14, where the aerostructural optimization goes over the trade-off between reducing airfoil thickness for aerodynamic benefits and mass reduction, and increasing it for structural stiffness.

The optimizer generally favored maximum thinning, leading to a higher suction peak at the front of the airfoil, which can be undesirable, especially near the wingtip, as thinner airfoils tend to stall abruptly. In the combined twist, chord, and shape optimization case, maximum airfoil thinning was achieved, but this resulted in excessive wing flexibility. In contrast, when all DVs are considered, the airfoil thickness reduction was comparably minimal, ensuring sufficient bending stiffness and maintaining the overall shape, with differences in pressure distribution reflecting variations in effective angle of attack.

In cases without the span variable, the optimizer significantly thinned wing panels, especially at the front spar and lower skin, while increasing the thickness of the upper skin near the root as seen in Fig. 15. This indicates a strategy to reduce thickness while reinforcing critical areas in response to changes in aerodynamic load. Conversely, allowing for span changes led to increased weight, with significant thickening of panels, particularly at the rear spar and lower skin near the root. This resulted in a 114% wing weight increase in the all DVs case, demonstrating that the sacrifice in range due to increased mass is outweighed by the reduction in induced drag, exacerbated by the absence of winglets.

The drastic improvement of the structural efficiency is attested by the KS index failure increase shown in Fig. 16, where the optimized wing box exhibits more regions with a higher failure index.

The ply angle distribution is shown in Fig. 17, indicating that the optimal solution is feasible for manufacturing with verified fiber continuity. The largest shifts in ply angles occur in sections with smaller safety factors, highlighting areas needing improvement. During flight, the main stresses involve bending the wing upward and twisting the airfoil. Consequently, fibers should be primarily aligned with the span direction to resist bending while being slightly tilted to manage shear forces from twisting which is verified.

5.4. Effect of the Aerostructural Analysis

The aerostructural analysis and optimization of a wing is computationally intensive, often taking significantly longer than isolated discipline analyses. Techniques like partial convergence help, but challenges remain due to the need for multiple partial, along with load and displacement transfers. The larger design space complicates matters, particularly with flawed mesh deformation techniques, which can lead to negative volumes under large loads and require artificial restrictive bounds. This complexity raises concerns about the time efficiency of obtaining the optimized solutions. There is a great difference when considering the computational time with a 12 threads CPU and clock speed of 4.5GHz. The structural analysis has a very low cost in the overall process, being concluded in just seconds (takes 99.95% less time than aerostructural), while there is a large cost for performing aerodynamic (less 66%) and aerostructural analysis, as multiples iteration between this two disciplines are needed. Moreover, the structural optimization converged in just 1.2 hours, while the aerodynamic optimization took nearly 26 hours. Finally, the aerostructural optimization stalled after approximately 140 hours (Tab. 5) due to the previous discussed reasons.

Table 5: Summary of Results for Each Type of Optimization

	A	S	AS
Mass	-	-70%	-44%
L/D	+3.1%	-	+14%
Run Time (h)	26	1.2	140
Memory Usage (GB)	16	8	40

Additionally, the accuracy of the prediction and the capturing of the aerostructural trade-offs is very visible in the optimal solution. Indeed, the structural optimization will achieve a much more efficient structure, as seen in the comparison between the thickness distribution present in Figures 18, having a much further reduction in mass of 70%, compared to 51% in the twist DV aerostructural case, with almost all the panels going to the minimal thickness allowed. That as an effect on the failure index passing from 0.55 to 0.35 and also in the wing deflection from 0.19 normalized deflection to 0.11 from the structural to the aerostructural cases.

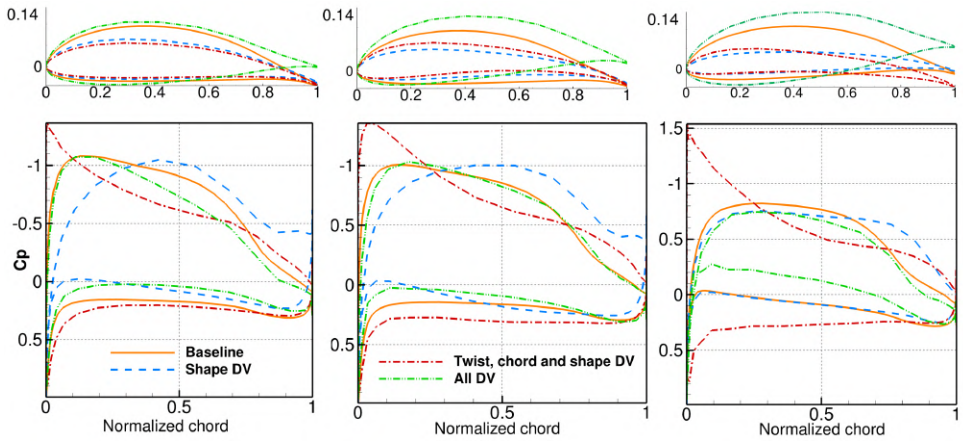

Figure 14: Airfoil shape and coefficient of pressure distribution at 10%, 50% and 90% of the span.

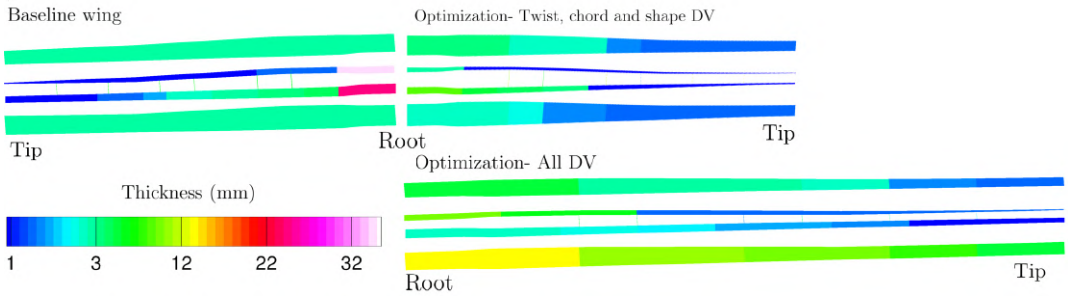

Figure 15: Thickness distribution in each optimization case.

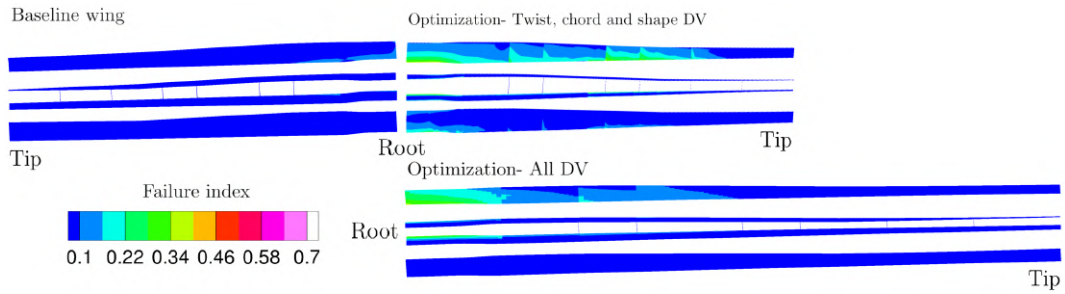

Figure 16: KS failure index in each optimization case.

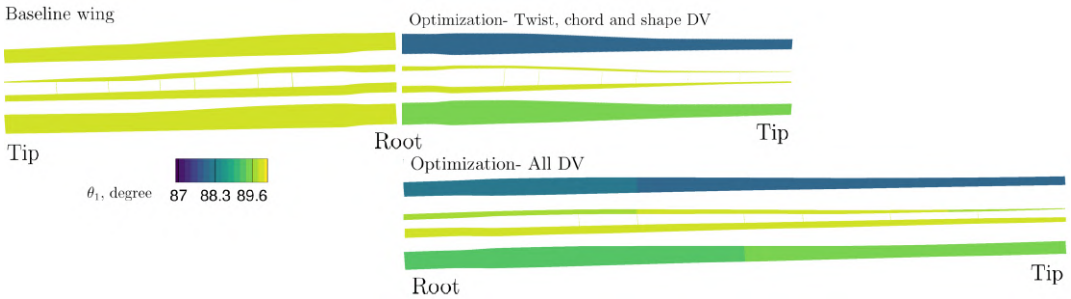

(a) Angle θ_1

Figure 17: Optimal distribution of ply angles in each optimization case.

This presents the problem that the deform wing could not produce the lift being required affecting the validity of the solution. Highlighting the advantage of considering the trade-off between the deflection and structural efficiency (until a certain point) and its consideration of the aerodynamic optimal in the overall solution.

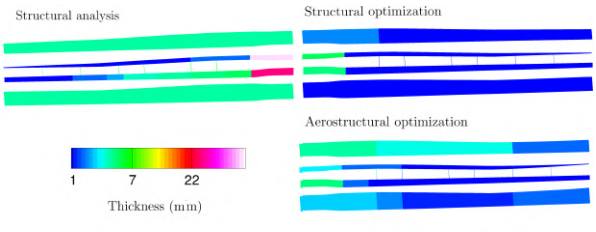

Figure 18: Thickness of structural material for aerodynamic/aerostructural analysis and optimization.

Aerodynamic optimization achieves an ideal elliptical lift distribution, but in the aerostructural solution, the lift shifts toward the wing root, reducing bending moments and highlighting the structural advantages of coupled analysis. Moreover, there is a clear tendency for the airfoil to thin under optimization, appearing the need to be constrained during the aerodynamic one, by an arbitrary thickness condition. This limitation is difficult to predict during the isolated optimization. The constraint being active, demonstrating the significant impact of including the structural weight in the objective function.

The airfoil thinning, results in an increase in deflection, reaching concerning values (around 0.28 normalized deflection) in contrast to the remaining cases therefor a deflection constraint still needs to be imposed. However, the thickness was still not directly limited. It was observed that even with the deflection constraint, there was a maximum thickness reduction of 14% (4% greater than at aerodynamic constraint).

The influence of structure on wing twist is evident in Fig: 19).

while aerodynamic optimization alone yields a more idealized twist, aerostructural analysis reveals deformation-induced positive twist under load, with tip twist increasing from 0° at jig, 2° in cruise to 9° in maneuvers. This confirms the importance of aerostructural analysis and stiffness constraints in shape DV cases to manage deflection and twist effectively.

While resource-intensive, the resulting improvements from the coupled aerostructural approach are substantial enough to demonstrate that such optimizations are necessary.

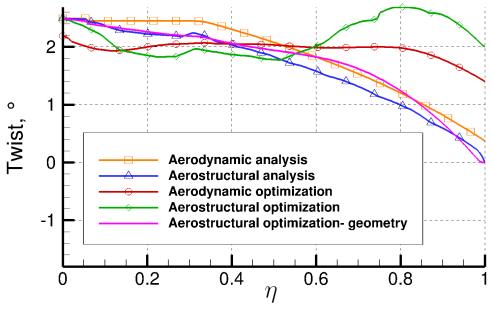

Figure 19: Twist distribution of the wing for aerodynamic/aerostructural optimization.

6. Conclusions

The study concluded that manufacturing constraints had a minimal effect on the final solution, while the deflection constraint was more impactful. When comparing aerodynamic, structural, and aerostructural optimizations, the aerostructural approach proved superior, despite taking 4.1 times longer since final solution differed substantially from individual discipline optimizations, offering a more balanced design that improved range.

From all cases studied, the optimizations led to a large decrease in mass, from 42.3% to 56.6%, while also allowed for an improvement in aerodynamic efficiency, from 0.6% to 32.2%. Moreover, progressively better results were shown with the all DV case resulting in an overall 9.9% increase in range.

Furthermore, the solution was less limited by failure constraints than initially expected. In all cases, the maximum value of 0.67 (from the 1.5 safety factor) was not reached, with the highest value achieved being around 0.45 in the cases involving twist, shape and chord design variables.

The most significant improvements were achieved by using span as a design variable, but the resulting 2.5m increase poses practical issues. The manufacturer noted that this large span would require a complete redesign, re-certification, and stricter regulation compliance, demanding more space, materials, labor, and complex molds to built. The larger wingspan complicates logistics and operations. Consequently, while span increase yields strong performance gains, it might be unfeasible for UAV wing redesign.

The twist, chord and shape DVs case with a displacement constraint a promising alternative , achieving a 4.2% range increase while preserving structural integrity. This a strong candidate for the informed design of the next TEKEVER AR5 iteration. showing no aeroelastic degradation even at diving speed and maximum loading factor presenting a smaller change in twist between the 1g and 2g cases.

At future work, the limitations of the current

mesh deformation algorithm should be addressed. Incorporate the full UAV geometry to better understand component interactions, buckling constraints should and refined material properties through experimental testing. Finally, access to more robust computing resources is essential to allow multipoint flight conditions, enabling the optimization process account for the complete flight envelope and complete UAV geometry.

References

[1] Gaetan K. W. Kenway, Graeme J. Kennedy, and Joaquim R. R. A. Martins. Scalable parallel approach for high-fidelity steady-state aeroelastic analysis and adjoint derivative computations. *AIAA Journal*, 52(5), 2014. doi:10.2514/1.J052255.

[2] Ruben Gameiro. Wing Aerodynamic Design for a MAME UAV using High-Fidelity Numerical Tools. Master's thesis, Instituto Superior Técnico, Portugal, 2023.

[3] Vitor Silva. Wing Structure Design for a MAME UAV using High Fidelity Numerical Tools. MSc Thesis in Aerospace Engineering, Instituto Superior Técnico, Portugal, 2023.

[4] MDO Lab of University of Michigan. MACH-Aero Framework. `https://mdolab-mach-aero.readthedocs-hosted.com`, 2023. (accessed on 2024-04-03).

[5] Ney R. Secco, Gaetan K. W. Kenway, Ping He, Charles Mader, and Joaquim R. R. A. Martins. Efficient mesh generation and deformation for aerodynamic shape optimization. *AIAA Journal*, 59(4):1151–1168, 2021. doi:10.2514/1.J059491.

[6] Charles A. Mader, Gaetan K. W. Kenway, Anil Yildirim, and Joaquim R. R. A. Martins. Adflow: An open-source computational fluid dynamics solver for aerodynamic and multidisciplinary optimization. *Journal of Aerospace Information Systems*, 17(9):508–527, 2020. doi:10.2514/1.I010796.

[7] Thomas W. Sederberg and Scott R. Parry. Free-form deformation of solid geometric models. In *SIGGRAPH '86: Proceedings of the 13th Annual Conference on Computer Graphics and Interactive Techniques*, New York, USA, August 1986. doi:10.1145/15922.15903.

[8] Gaetan Kenway, Graeme Kennedy, and Joaquim R. R. A Martins. A CAD-free approach to high-fidelity aerostructural optimization. Texas, USA, oct 2010. doi:10.2514/6.2010-9231.

[9] J. N. Reddy. *Mechanics of Laminated Composite Plates and Shells: Theory and Analysis*. CRC Press, 2nd edition, 2003. ISBN 9780849315923.

[10] Ruben Perez, Hugh Liu, and Kamran Behdinan. Evaluation of multidisciplinary optimization approaches for aircraft conceptual design. In *10th AIAA/ISSMO multidisciplinary analysis and optimization conference*, Albany, USA, August 2004. doi:10.2514/6.2004-4537.

[11] Graeme J. Kennedy and Joaquim R.R.A. Martins. A parallel finite-element framework for large-scale gradient-based design optimization of high-performance structures. *Finite Elements in Analysis and Design*, 87, 2014. doi:10.1016/j.finel.2014.04.011.

[12] Graeme Kennedy and Joaquim R. R. A Martins. A parallel finite-element framework for large-scale gradient-based design optimization of high-performance structures. *Finite Elements in Analysis and Design*, 87:56–73, oct 2014. doi:10.1016/j.finel.2014.04.011.

[13] Donald R. Askeland, Pradeep P. Fulay, and Wendelin J. Wright. *The Science and Engineering of Materials*. Cengage Learning, 6th edition, 2010. ISBN:9780495296027.

[14] Ali. Khani, Samuel T. IJsselmuiden, M. M. Abdalla, and Z. Gürdal. Design of variable stiffness panels for maximum strength using lamination parameters. *Composites Part B Engineering*, 42(3), 2011. doi:10.1016/j.compositesb.2010.11.005.

[15] Zhoujie Lyu, Zelu Xu, and J. R. R. A. Martins. Benchmarking optimization algorithms for wing aerodynamic design optimization. In *Proceedings of the 8th International Conference on Computational Fluid Dynamics*, Chengdu, China, July 2014. ICCFD8-2014-0203.

[16] Ella Wu, Gaetan Kenway, Charles A. Mader, John Jasa, and Joaquim R. R. A. Martins. pyoptsparse: A python framework for large-scale constrained nonlinear optimization of sparse systems. *Journal of Open Source Software*, 5 (54):2564, 2020. doi:10.21105/joss.02564.

[17] Joaquim R. R. A. Martins and Graeme Kennedy. Enabling large-scale multidisciplinary design optimization through adjoint sensitivity analysis. *Structural and Multidisciplinary Optimization*, 64, 2021. 10.1007/s00158-021-03067-y.